Nigel and the optical sky brightness at Dome C, Antarctica

Suzanne L. Kenyon*, Michael C. B. Ashley, Jon Everett, Jon S. Lawrence and John W. V. Storey

School of Physics, University of New South Wales, Sydney 2052, Australia

ABSTRACT

The brightness of the night sky at an astronomical site is one of the principal factors that determine the quality of available optical observing time. At any site the optical night sky is always brightened with airglow, zodiacal light, integrated starlight, diffuse Galactic light and extra-galactic light. Further brightening can be caused by scattered sunlight, aurorae, moonlight and artificial sources. Dome C exhibits many characteristics that are extremely favourable to optical and IR astronomy; however, at this stage few measurements have been made of the brightness of the optical night sky. Nigel is a fibre-fed UV/visible grating spectrograph with a thermoelectrically cooled 256×1024 pixel CCD camera, and is designed to measure the twilight and night sky brightness at Dome C from 250 nm to 900 nm. We present details of the design, calibration and installation of Nigel in the AASTINO laboratory at Dome C, together with a summary of the known properties of the Dome C sky.

Keywords: Site testing, Antarctica, sky brightness

1. INTRODUCTION

Dome C, Antarctica ($75°6'$ south, $123°21'$ east, 3250 m) has been recognised as a promising optical and infrared astronomical site for a number of years.[1] Above a thin boundary layer the atmospheric turbulence is very weak, leading to exceptionally good seeing. Measurements of the turbulence using a MASS and a SODAR in winter 2004 showed an average seeing above 30 m of $0.27''$, with the seeing better than $0.15''$ for 25% of the time.[2] These results were independently confirmed in winter 2005; DIMM measurements showed an average seeing of $0.25''$ above the ground layer with 87% of the turbulence confined to the first 36 m of the atmosphere.[3] The extremely cold temperatures and low precipitable water vapour at Dome C also result in an infrared sky background that is very much lower than at temperate sites.[4]

To date the optical sky brightness of Dome C has not been monitored during the winter. Because of the high latitude of Dome C, the Sun spends a relatively small amount of time a long way below the horizon, resulting in long periods of twilight. There is thus a need to evaluate both the quality and quantity of dark time at Dome C. Nigel is a spectrograph designed to measure both the optical twilight and the nighttime sky brightness at Dome C. Nigel was installed in the AASTINO (Automated Astrophysical Site Testing International Observatory[5]) in November 2004 and collected data until 13 February 2005.

In Section 2 we discuss the various contributions to sky brightness at Dome C and discuss the amount of usable dark time. In Section 3 we discuss the aims, design and installation of Nigel. Finally, in Section 4 we summarise future plans for Nigel.

2. SKY BRIGHTNESS

The sky is never completely dark in optical wavelengths. At the darkest sites, long after sunset, the sky background is on the order of 22.0–21.1 V mag arcsec^{-2} at zenith.[6] Sky brightening is caused by sunlight, moonlight, airglow, aurorae, zodiacal light, integrated starlight, diffuse Galactic light, extra-galactic light and artificial sources. Kenyon & Storey (2006)[7] present a detailed analysis of the sky brightness at Dome C and provide a comparison to Mauna Kea, Hawaii. In this section we summarise the main conclusions of that paper.

* suzanne@phys.unsw.edu.au

Ground-based and Airborne Telescopes, edited by Larry M. Stepp, Proc. of SPIE
Vol. 6267, 62671M, (2006) · 0277-786X/06/$15 · doi: 10.1117/12.672362

Sunlight No direct sunlight reaches the surface of the Earth after sunset, however, sunlight is *scattered* off atmospheric molecules and aerosol particles towards the surface. This is the highest contributor to sky brightness until the Sun is about 8° below the horizon. Scattering from atmospheric molecules is essentially the same at all sites of similar elevation, so little advantage is expected at Dome C in this respect. However, aerosol scattering is extremely variable between sites. Because of the extremely clear atmosphere at Dome C it is expected that aerosol scattering will be minimal. No measurements of aerosols have been taken at Dome C, however the annual average scattering coefficient at South Pole is 5 times less than at Mauna Loa, Hawaii.[8,9] The main aerosol in the atmosphere at South Pole is sea salt that has been transported from the coast. As Dome C is further from the coast than South Pole, it is expected that the aerosol content of the atmosphere there will be even lower. Astronomical nighttime is formally defined to begin when the Sun reaches a depression angle of 18°. Using this definition, Dome C has about 50% the dark-time of Mauna Kea. When the cloud cover at each site is taken into account, however, it appears that Dome C may have a comparable number of cloud-free dark hours to Mauna Kea.

Moonlight Moonlight brightens the sky in much the same way as the Sun, by direct transmission and scattering. At Dome C, the maximum elevation of the Moon ranges between about 33° and 43° over the 18 yr lunar nodal cycle. At sites closer to the equator, such as Mauna Kea, the Moon can always pass through the zenith, regardless of the lunar nodal cycle. Models of the sky brightening caused by the Moon show that, averaged over the epoch 2005–2015, moonlight brightens the sky at zenith by a median value of 1.7 V mag arcsec^{-2} at Dome C, and 2.1 V mag arcsec^{-2} at Mauna Kea.[7]

Aurorae Aurorae are caused by the collisions of highly energetic solar particles with upper atmosphere atoms and molecules. The collisions excite the atoms and molecules to higher energy states, from which they radiatively decay. Dome C is about 10° from the inner edge of the southern auroral oval; aurorae are therefore expected to be low on the horizon and of low intensity. Using geometric calculations, aurorae at Dome C are generally expected to be lower than 7° elevation and 1100–2000 km away.

Airglow Airglow, at night, is the chemiluminescence of upper atoms and molecules. Airglow emissions in the visible are shown in Table 1. In general, little difference in overall airglow emission between Antarctic and temperate sites is expected.

Table 1. Airglow emissions at zenith in the visible range [7, and ref. therein].

Wavelength (nm)	Source	Height (km)	Typical intensity (R)
260 – 380	O_2	90	0.5 Å^{-1}
500 – 650	NO_2	90	250
519.8, 520.1 1	N	1	
557.7	OI	95	250
557.7	OI	250 – 300	20
589.0, 589.6	Na D	$\sim$ 92	50
600 – 4500	OH	85	4500 k
630.0	OI	250 – 300	100
636.4	OI	250 – 300	20
761.9	O_2	$\sim$ 80	1000
864.5	O_2	$\sim$ 80	1000

Zodiacal light Zodiacal light is caused by sunlight scattering from the diffuse cloud of interplanetary dust that lies in the plane of the solar system. Models of the zodiacal light at Dome C show it is expected to be always darker than 23.1 V mag arcsec^{-2}, at zenith. Similar models for Mauna Kea estimate the zodiacal light to be always brighter than 23.1 V mag arcsec^{-2}. The reduced zodiacal light at Dome C is not a characteristic of the site per se, but rather due to the different parts of the sky that are observed, i.e., the zodiac is always lower on the horizon at Dome C.

Integrated starlight Integrated starlight is from all the stars fainter than the limiting magnitude of the telescope. The limiting magnitude of even a small telescope at Dome C should be dark enough for the integrated starlight to be reduced to negligible levels.

Diffuse Galactic light Diffuse Galactic light is starlight scattered off interstellar dust. Diffuse Galactic light is typically about 23.6 V mag arcsec^{-2} at zenith.[10] The Galactic plane is always close to the zenith at Dome C and this may result in a relatively higher contribution of diffuse Galactic light and integrated starlight, compared to lower latitude sites. This contribution is rather smaller than other sources of sky brightness and, similarly to zodiacal light, depends on the celestial coordinates.

Integrated cosmic light Integrated cosmic light is the redshifted starlight from unresolved galaxies. This contribution, at all sites, is very small compared to other sources of sky brightness, and is expected to be in the range of 25–30 mag arcsec^{-2} at 550 nm.[6]

Artificial sources The night sky can be brightened considerably by light pollution from towns and cities. At Dome C, light pollution from other stations will not be a problem; the nearest station (Vostok) is about 560 km away. With thoughtful planning in regards to external lighting at Dome C there should be no artificial light pollution, whereas the light pollution at other astronomical observatories, with close-by towns, is likely to increase.

3. NIGEL

Nigel is a fibre-fed spectrograph for the measurement of the optical brightness, temporal characteristics and spectrum of the twilight and nighttime sky, including auroral events. Nigel was developed from the Antarctic Fibre Optic Spectrograph (AFOS)[11] which operated at the South Pole from 2002–2003.[12] Nigel was installed in the AASTINO at Dome C in November 2004, and operated until 13 February 2005, at which time the entire AASTINO system was shut down. Unfortunately this means that the darkest sky we recorded was when the Sun was barely below the horizon.

In this section we describe the instrument design, installation and calibration.

3.1. Instrument Design

Nigel has six optical fibres that collect light from three directions in the sky and direct it into a spectrograph; the resulting image is recorded on a CCD. The spectrograph, CCD and control computer were located inside the AASTINO and the fibres fed outside through a roof port. Nigel is designed to operate in the wavelength range 250 nm–900 nm, so to ensure good efficiency over the whole spectral range we used two sets of fibres, optimised in red and blue wavelength ranges. Both sets of fibres were supplied by Ceramoptec and have a standard numerical aperture of 0.22 ± 0.02 with a core diameter of 100 μm. The 6 fibres are paired into blue and red optimised combinations. The fibre numerical aperture corresponds to an f-ratio of $f/2.2$; each fibre thus sees a field of view of 25° on the sky. Each pair of fibres was pointed in a different direction, one pair towards the zenith and the other two pairs elevated to 30° and pointed in northerly and southerly directions.

The "sky" end of each fibre is held in an SMA connector, with a coaxial copper tube to hold the fibres in place on the top of the AASTINO. The tube can be electrically heated to prevent ice build up near the fibres. Each fibre is threaded into Teflon tubing for protection; Teflon was chosen as it remains flexible at the cold temperatures

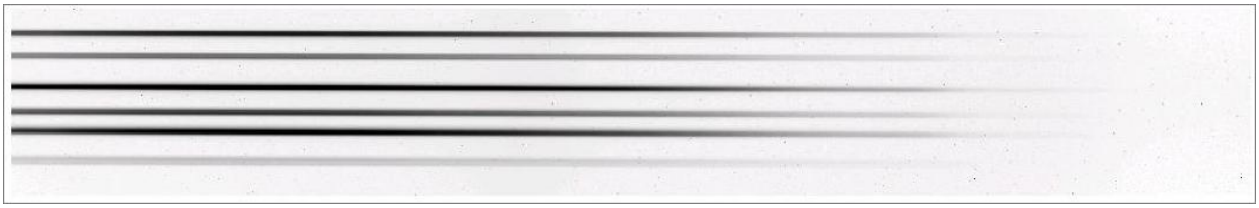

Figure 1. Raw CCD image taken with Nigel. Each horizontal line corresponds to the spectrum from one fibre; wavelength decreases to the right.

experienced at Dome C. Inside the AASTINO the tubes were bundled together and threaded into a rubber tube for further protection. The spectrograph end of the fibres is held in a brass connector. The connector is machined with six parallel and evenly spaced V-grooves. Each fibre was glued into a groove and cut flush with the edge of the connector. The resulting linear array of fibres forms a pseudo-slit to the spectrograph, with the spectrum from each fibre separated by about 20 pixels on the spectrograph. The fibre ends were hand-polished.

We used a commercial spectrometer (Jobin Yvon model CP200). The grating is concave holographic and produces a linear dispersion that varies from 24.6 nm/mm in the blue to 25.7 nm/mm in the red. With the 100 μm fibres, the resulting resolution is 2.5 nm full width half maximum. The 1024×256 pixel CCD camera was an Andor unit supplied by Oriel Instruments (model Instaspec IV, open electrode) and is cooled by a single air-cooled Peltier stage. With a wavelength range of 250–900 nm spread across the 1024 pixel CCD camera, each resolution element is spread across about 4 pixels. The images on the CCD are saved in the FITS file format. Figure 1 shows a CCD image taken with Nigel; each horizontal line corresponds to the spectrum from one fibre, and the wavelength decreases to the right.

3.2. Control

Ultimate control over the operation of Nigel is by the "Supervisor" computer in the AASTINO. The Supervisor controls the power and heat in the AASTINO as well as the operation of various instruments and communications. Communications to the Supervisor from off-site are via the Iridium satellite network. Nigel has a separate PC104 computer to control the CCD. The two computers are connected via ethernet and communicate using the ERIC software package.[13]

The observing sequence of Nigel is controlled by a Perl script on the Supervisor that automatically starts each day by a crontab file. This script controls the frequency of exposures and the exposure times, depending on the azimuth and altitude of the Sun and Moon, and the phase of the Moon. If the Sun is in the field of view of a pair of fibres no exposure is taken. If the Moon is in the field, then exposures are taken every 15 minutes, otherwise every 3 hours. The number of exposures taken is limited by the storage capacity available, when compressed each FITS file is about 125 KBytes in size. If an exposure is to be taken, a shell script is started that communicates and controls the CCD computer, including cooling the CCD, setting the read out area and time and taking the exposure. All exposures are saved on the Supervisor and timestamped.

3.3. Calibration

3.3.1. Wavelength calibration

The wavelength scale of the spectrograph was initially calibrated using a domestic fluorescent light tube. The tube of a fluorescent light contains a rare gas (usually Argon) and a small amount of mercury. The tube is coated on the inside with phosphor. Typically a combination of three rare earth phosphors is used, emitting in the red (e.g. Y_2O_3:Eu^{3+}), green (e.g. $CeMgAl_{11}O_{19}$: Tb^{3+}, $LaPO_4$:Ce^{3+},Tb^{3+}, $GdMgB_5O_{10}$:Ce^{3+},Tb^{3+}) and blue (e.g. $BaMgAl_{10}O_{17}$:Eu^{2+}, $(Sr,Ba,Ca)_5(PO_4)_3$:Eu^{2+}).[14,15] Table 2 shows the nominal wavelengths and probable identifications of each fluorescent peak used for wavelength calibration.

Additional wavelength calibration was from known Fraunhofer absorption lines in daytime sky spectra. Figure 2 shows a fluorescent and daytime sky spectrum taken with Nigel, with the calibration lines marked.

Table 2. Probable identification of fluorescent lines[16–19]

Peak label	Nominal wavelength (nm)	Probable identification	Peak label	Nominal wavelength (nm)	Probable identification
a	405	Hg I	i	625	Tb IV $^5D_4 \rightarrow ^7F_3$
b	436	Hg I	j	631	Eu IV $^5D_0 \rightarrow ^7F_3$
c	488	Tb IV $^5D_4 \rightarrow ^7F_6$	k	651	Eu IV $^5D_0 \rightarrow ^7F_3$
d	544	Tb IV $^5D_4 \rightarrow ^7F_5$	l	662	?
	546	Hg I	m	688	Eu IV $^5D_0 \rightarrow ^7F_4$
e	588	Eu IV $^5D_0 \rightarrow ^7F_1$	n	694	Eu IV $^5D_0 \rightarrow ^7F_4$
f	594	Tb IV $^5D_4 \rightarrow ^7F_4$	o	708	?
g	599	Eu IV	p	742	Eu IV $^5D_0 \rightarrow ^7F_5$
h	611	Eu IV $^5D_0 \rightarrow ^7F_2$	q	809	Eu IV $^5D_0 \rightarrow ^7F_6$

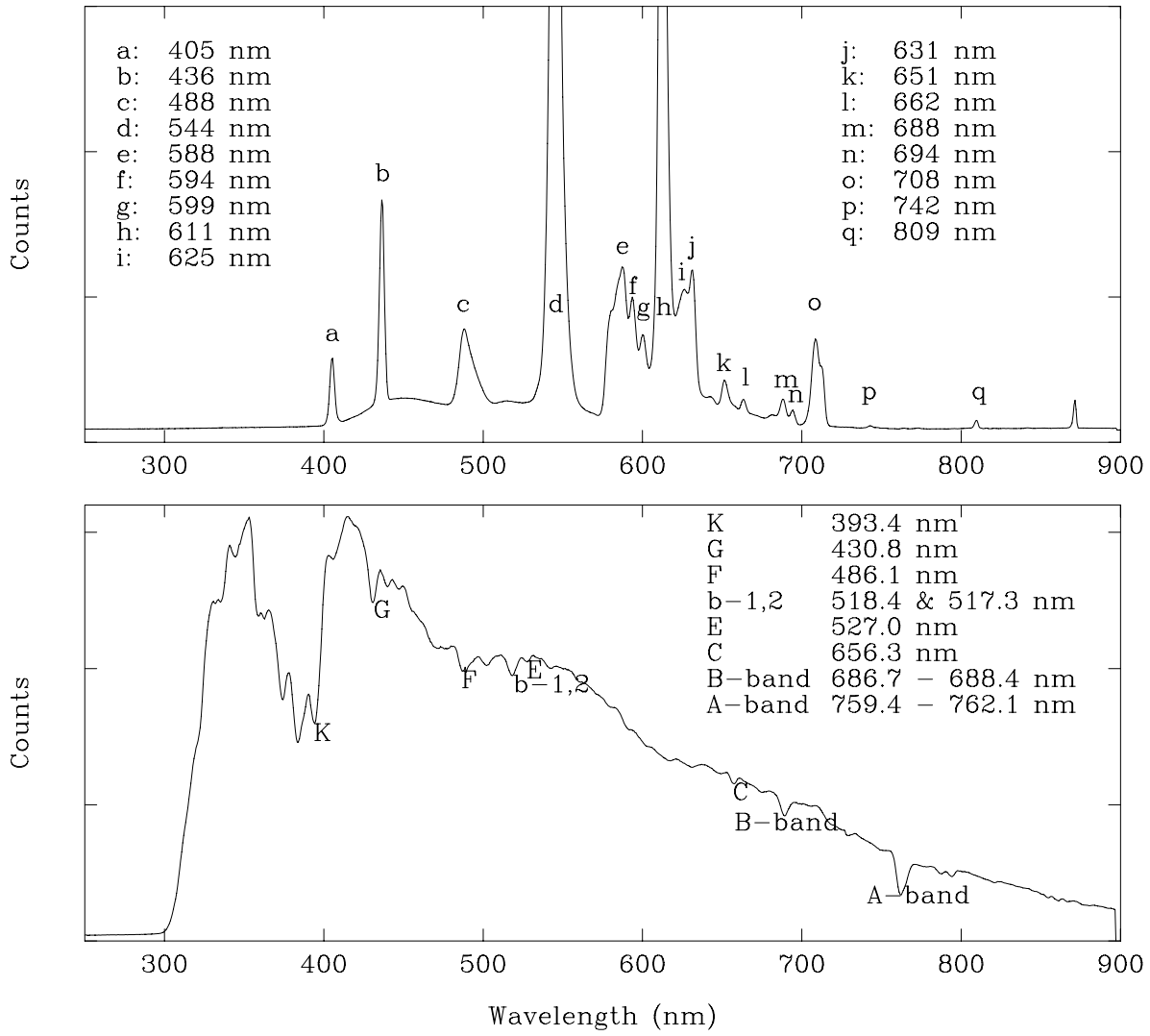

Figure 2. Spectrum of a compact fluorescent tube (*top)* and the daytime sky *(bottom)* showing the calibration wavelengths.

3.3.2. Flux calibration

To achieve an absolute flux calibration of Nigel we explored a method using light from a tungsten bulb reflected off a diffuse white surface.[20,21] We also planned to use lunar spectra to check the flux calibration during the year, as the Moon would pass through the field of view of all but the zenith fibres on several occasions.

The idea behind the first method is to illuminate a Lambertian surface with a tungsten globe and observe the reflected light with the spectrograph. The spectral luminance (photons $s^{-1}m^{-2}sr^{-1}(m)^{-1}$) of the Lambertian surface can be calculated from

$$B(\lambda, T) = a_f E(\lambda, T)\alpha(\lambda)\frac{1}{4\pi^2 L^2}\cos\theta, \tag{1}$$

where λ is the wavelength; T, a_f and $E(\lambda, T)$ are the temperature, area and spectral emittance of the filament; $\alpha(\lambda)$ is the albedo of the surface, L is the distance between the filament and the surface, and θ is the angle between the filament and the normal to the Lambertian surface. The temperature of the bulb is estimated from the known temperature–resistivity relationship for tungsten. The surface area of the filament is calculated from the power, total emissivity and temperature.

Because of the large wavelength range, we have to take into account light from wavelengths between 245 and 450 nm that will pass through the grating in the second order and contaminate the wavelength range 490 – 900 nm. To account for this we took calibration images with and without a 515 nm long-pass glass filter in front of the fibres.

Figures 3a and 3b show the response of the system to the illuminated Lambertian screen, unfiltered and filtered with a long-pass 515 nm filter, respectively. Figures 3c and 3d show the same data, but with the intensity axis zoomed in to show the behaviour at short wavelengths. These plots show that even in the filtered case, the intensity does not drop to zero at shorter wavelengths but has a pedestal of about 215 counts per second. This is probably caused by scattering within the spectrometer. On average this pedestal accounts for about 5×10^{-5} of the total flux recorded in a fibre, close to the expected stray light rejection ratio of 10^{-4}. We calculated the expected output from the tungsten globe using Equation (1), this spectrum is shown as the dashed line in Figures 3a and 3b.

After removing the scattered light contribution (assumed to be a constant 215 counts per second) from the measured spectra, we took the ratio between the measured response and the tungsten spectrum (see Figures 3e and 3f). Also plotted is the transmission expected from the quantum efficiency of the CCD[22] convolved with the grating efficiency.[23] The system transmission we obtain for the "best" fibre agrees reasonably well both in shape and in absolute terms with the expected transmission at all wavelengths longer than about 500 nm. However, the absolute transmission of the other fibres is considerably less. This is probably because of bad coupling efficiency between the fibre ends and the grating, possibly a result of the polishing technique, or the fibre ends could have been damaged in transit.

As shown in Figure 3e, this technique of flux calibration becomes unreliable at short wavelengths because the flux radiated from the bulb is too weak and the response becomes dominated by scattered light. In addition, the glass bulb will be absorbing some UV light.[21]

Figure 4 shows the measured transmission of each fibre, divided by the transmission through the brightest fibre F_4. Each ratio is fairly constant, showing that as a means of calibrating the transmission between each fibre, this method is quite useful.

3.3.3. Conclusions on calibration methods

We found that the incandescent bulb method can potentially be used for absolute flux calibration at visible and near infrared wavelengths. If delicate calibration standards cannot be taken into the field with the instrument, careful calibration could be carried out in a laboratory and this method could be used to check the calibrations in the field. Coupled with the wavelength calibration using a fluorescent bulb, this incandescent bulb method is a cheap and easy way to test the calibration. This technique could be improved by using a hotter filament in conjunction with a short-pass filter, although at very short wavelengths absorption of UV by the glass bulb becomes a problem.

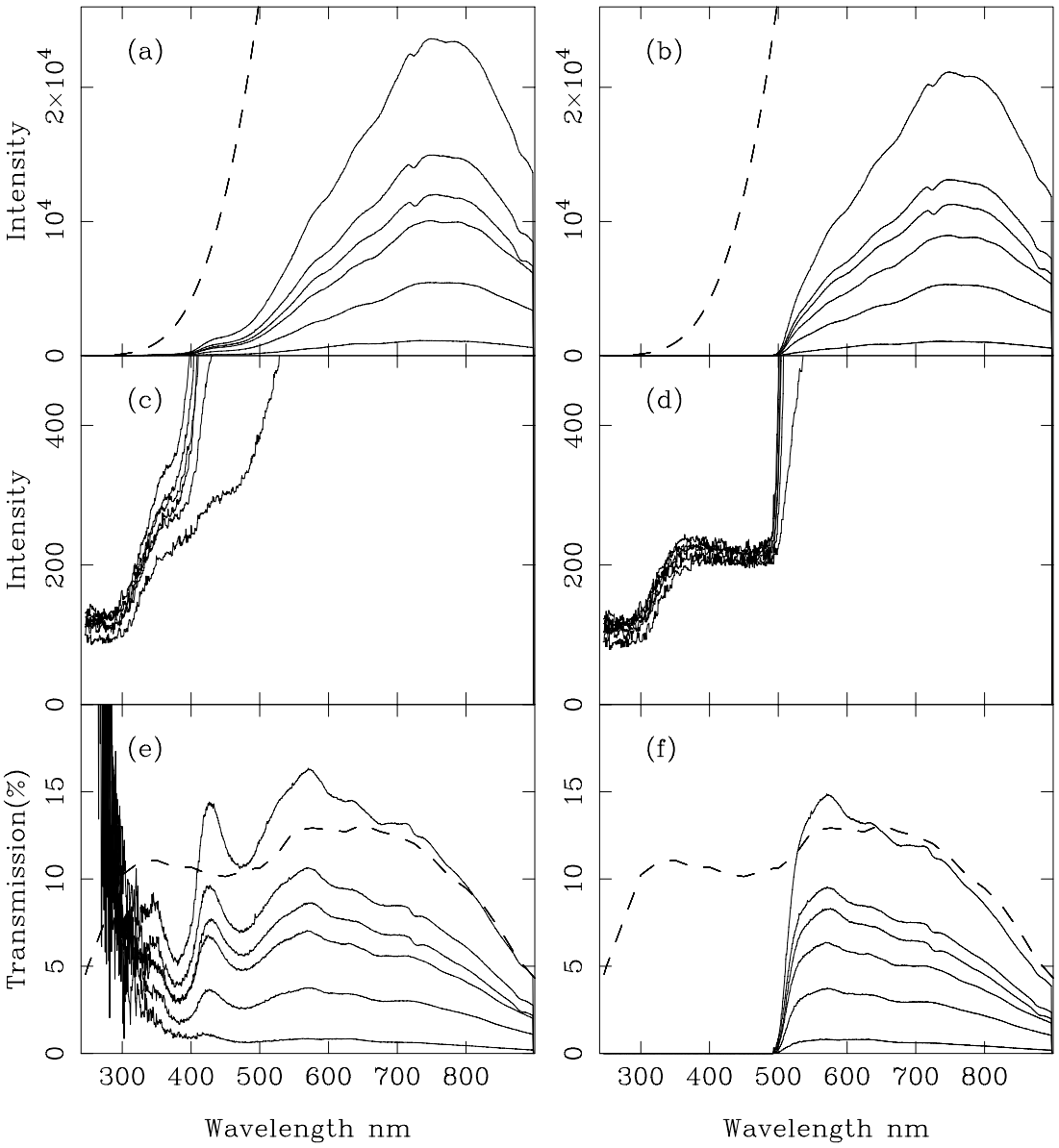

Figure 3. *(a)* Intensity as a function of wavelength for an exposure of the Lambertian screen without a filter and *(b)* with a 515 nm long-pass filter; the solid lines show the measured response through each of the six fibres and the dashed line shows the calculated emission from the tungsten filament. Plots *(c)* and *(d)* are the same, with the intensity axis zoomed in. Plots *(e)* and *(f)* show the ratio of the measured response to the tungsten spectrum, for the unfiltered and filtered set-ups, respectively. Also shown (dashed) is the expected quantum efficiency of the CCD convolved with the grating efficiency. In all cases the order of fibres from brightest is F_4, F_2, F_6 (red), then F_3, F_5 and F_1 (blue).

4. DISCUSSION AND NIGEL'S PLANS FOR THE FUTURE

The large field of view (25°) of Nigel will mean that at times when the Galactic plane is passing through the field, the contribution from starlight will be comparatively large. This means that each measurement needs to be carefully analysed according to what part of the sky is being observed. In this respect Nigel is an ideal companion instrument to the Gattini-Sky Background (Gattini-SBC) and Gattini-All Sky cameras,[24] currently in operation at Dome C. The Gattini-SBC is designed to measure the optical sky brightness between the stars

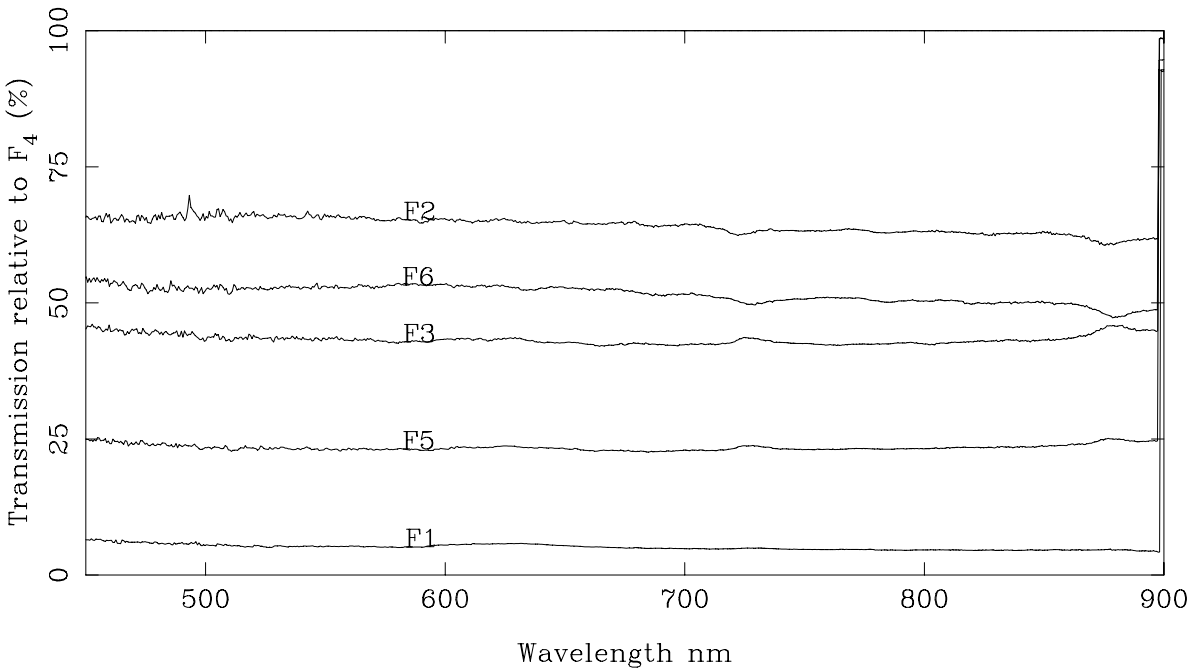

Figure 4. Measured transmission of each fibre relative to the brightest fibre (F_4). Most of the difference is probably due to coupling losses at the ends of the fibres.

in a 6° by 4° field centred on the South Pole. Gattini-SBC will also pick up auroral events, and combination of these data with spectra from Nigel would allow these events to be identified. Using the spectra from Nigel we may also be able to identify periods of cloud cover. Twilight spectra from Nigel will be useful for analysis of the profile of the atmosphere, and could be compared to similar measurements at ESO-Paranal.[25]

Nigel was removed from Dome C during the summer 2005/2006 season and returned to Sydney. The instrument will be upgraded and sent to either Dome C for the 2007 winter or to Dome A for the 2008 winter. Before redeployment we plan to upgrade the fibres and connectors, and include an inline long-pass filter on each of the red fibres to eliminate second order contamination from the shorter wavelengths. We will also further improve the calibration system, including careful tests on the absolute flux calibration method outlined above. If the instrument is deployed to Dome A, we will need to ensure it is completely autonomous and may need to include a system to test the calibration throughout the year. Dome C is now manned all year around and the calibration could be regularly checked by the winterover person in charge of the site testing experiments. Before redeployment the upgraded Nigel will be tested at an observatory in Australia to test the response to the night sky brightness and to refine the data reduction process; in addition, we may test Nigel at another high latitude site to assess the response to aurorae.

ACKNOWLEDGMENTS

We would like to thank the Australian Research Council and the Australian Antarctic Division for financial support, and the French (IPEV) and Italian (PNRA) Antarctic programs for logistical support. We thank our colleagues from the University of Nice for their assistance when we were setting up the experiment at Dome C. SLK is supported by an Australian Postgraduate Award and by an Australian Antarctic Division top-up scholarship.

REFERENCES

1. J. W. V. Storey, M. C. B. Ashley, J. S. Lawrence, and M. G. Burton, "Dome C—the best astronomical site in the world?," *Mem. Soc. Astron. Ital. Suppl.* **2**, pp. 13–18, 2003.

2. J. S. Lawrence, M. C. B. Ashley, A. Tokovinin, and T. Travouillon, "Exceptional astronomical seeing conditions above Dome C in Antarctica," *Nature* **431**, pp. 278–281, 2004.
3. A. Agabi, E. Aristidi, M. Azouit, E. Fossat, F. Martin, T. Sadibekova, J. Vernin, and A. Ziad, "First whole atmosphere night-time seeing measurements at Dome C, Antarctica," *Publ. Astron. Soc. Pac.* **118**, pp. 344–348, 2006.
4. V. P. Walden, M. S. Town, B. Halter, and J. W. V. Storey, "First measurements of the infrared sky brightness at Dome C, Antarctica," *Publ. Astron. Soc. Pac.* **117**, pp. 300–308, 2005.
5. J. S. Lawrence, M. C. Ashley, and J. W. V. Storey, "A remote, autonomous laboratory for Antarctica with hybrid power generation," *Aust. Journal Elec. & Electronic Eng.* **2**, pp. 1–12, 2005.
6. C. Leinert, S. Bowyer, L. K. Haikala, M. S. Hanner, M. G. Hauser, A.-C. Levasseur-Regourd, I. Mann, K. Mattila, W. T. Reach, W. Schlosser, H. J. Staude, G. N. Toller, J. L. Weiland, J. L. Weinberg, and A. N. Witt, "The 1997 reference of diffuse night sky brightness," *Astron. Astrophys. Suppl. Ser.* **127**, pp. 1–99, 1998.
7. S. L. Kenyon and J. W. V. Storey, "A review of optical sky brightness and extinction at Dome C, Antarctica," *Publ. Astron. Soc. Pac.* **118**, p. 489, 2006.
8. E. Andrews, D. Jackson, A. Jefferson, S. Kim, J. Ogren, P. Sheridan, and J. Wendell, "Aerosols and radiation: Aerosol monitoring," in *CMDL Summary Report #27*, A. McComiskey, ed., pp. 58–66, CMDL, 2002-2003.
9. B. A. Bodhaine, "Aerosol absorption measurements at Barrow, Mauna Loa and the South Pole," *J. Geo. Res.* **100**, pp. 8967–8976, 1995.
10. F. E. Roach and J. L. Gordon, *The Light of the Night Sky*, D.Reidel Publishing Company, Dordrescht, Holland, 1973.
11. M. Boccas, M. C. B. Ashley, A. Phillips, A. Schinckel, and J. W. V. Storey, "Antarctic Fiber Optic Spectrometer," *Publ. Astron. Soc. Pac.* **110**, pp. 306–316, 1998.
12. J. T. Dempsey, J. W. V. Storey, M. C. B. Ashley, M. G. Burton, P. G. Calisse, and M. A. Jarnyk, "AFOS: probing the UV-visible potential of the Antarctic plateau," *Proc. SPIE* **5492**, pp. 811–821, 2004.
13. M. C. B. Ashley, P. W. Brooks, and J. P. Lloyd, "Remote control of astronomical instruments via the Internet," *Publ. Astron. Soc. Aust.* **13**, pp. 17–21, 1996.
14. A. Srivastava and T. Sommerer, "Fluorescent lamp phosphors," *The Electrochemical Society Interface* **7**, pp. 28–31, 1998.
15. Dejneka, M. J., et. al, "Rare earth-doped glass microbarcodes," *Publ. Natl. Acad. Sci USA* **100**, pp. 389–393, 2003.
16. G. Ofelt, "Structure of the f6 configuration with application to rare-earth ions," *J. Chem. Phys.* **38**, pp. 2171–2180, 1963.
17. L. G. DeShazer and G. H. Dieke, "Spectra and energy levels of Eu^{3+} in $LaCl_3$," *J. Chem. Phys.* **38**, pp. 2190–2199, 1963.
18. L. Thompson, O. A. Serra, J. P. Riehl, F. S. Richardson, and R. W. Schwartz, "Emission spectra of $Cs_2NaTbCl_6$ and Cs_2NaYCl_6: Tb^{3+}," *Chem. Phys.* **26**, pp. 393–401, 1977.
19. J. Koningstein, "Energy levels and crystal-field calculations of europium and terbium in yttrium aluminum garnet," *Phys. Rev.* **136**, pp. A717–A725, 1964.
20. O. Harang and M. Kosch, "Absolute optical calibrations using a simple tungsten bulb: theory," *Sodankylä Geophysical Observatory Publications* **92**, pp. 121–123, 2003.
21. O. Harang. private communication, 2004.
22. Oriel Instruments, *Catalog, New Products for Light Research*, 1995.
23. Jobin Yvon, *CP 200 Technical Manual*, 1989.
24. A. Moore, E. Aristidi, M. C. B. Ashley, M. Candidi, J. Everett, S. L. Kenyon, J. S. Lawrence, A. Phillips, B. Le Rouxe, R. Ragazzonie, P. Salinarie, J. W. V. Storey, M. Taylor, and T. Travouillon, "The Gattini cameras for optical sky brightness measurements in Antarctica," *these proceedings* , 2006.
25. F. Patat, O. Ugolnikov, and O. Postylyako, "UBVRI twilight sky brightness at ESO-Paranal," *Astron. Astrophys., in press* , 2006.